Paper presented at the 22nd Asian Conference on Remote Sensing, 5 - 9 November 2001, Singapore.

EXPANSION OF THE UNSUPERVISED CLASSIFICATION OF POLARIMETRIC SAR IMAGES BASED ON THE SCATTERING TYPES USING THE SHAPE FEATURES OF POLARIZATION SIGNATURE DIAGRAMS

Takahiro YAMADA
Graduate School of Science and Engineering,
Ibaraki University
4-12-1 Nakanarusawa, Hitachi, Ibaraki, 316-8511, Japan
Tel: (81)-294-38-8235, Fax: (81)-294-38-5282
E-mail: yamada@fukushima-nct.ac.jp

Takashi HOSHI
Professor, Department of the Computer and Information Sciences,
Faculty of Engineering, Ibaraki University
4-12-1 Nakanarusawa, Hitachi, Ibaraki, 316-8511, Japan
Tel: (81)-294-38-5133, Fax: (81)-294-38-5282
E-mail: hoshi@cis.ibaraki.ac.jp

KEY WORDS: Land-cover Classification, Polarization Signature Diagrams, SIR-C

ABSTRACT: Various algorithms of supervised or unsupervised classification processing have proposed for polarimetric SAR image data. J. J. van Zyl proposed an unsupervised classification algorithm that was one of representative methods based on the scattering mechanism of microwave. In this method, each target is classified using information based on Mueller matrices of the targets into three scattering types. In this study, we introduced the shape features of polarization signature diagram used as a tool for the polarimetric SAR data, and supplemented classes. Applying this proposed method to SIR-C data, some targets confused in the same class could be classified into the separate supplemented class.

1. INTRODUCTION

Polarimetric SAR observes the surface using multiple-polarization microwave, and various examples for geo-science applications have been reported [1]-[4]. Many supervised or unsupervised classification methods have been proposed for land-cover classification, and their effectiveness has been confirmed [5]-[7].

The classification based on the scattering mechanism proposed by J. J. van Zyl is a representative method for unsupervised classification using polarimetric SAR data, and some applications have been reported [8][9]. In this method, targets are classified to four classes constructed by three scattering types, odd number of reflections, even number of reflections, and diffuse scattering, and the others labeled "not classified," so that different targets often classified the same class. For example, urban area and paddy field are classified to even number of reflections class when L-band data are used.

In this study, we tried to classify each class more closely by introducing the information of the shape of polarization signature diagram to avoid the confusion. As the shape information, we use the position where back-scattering coefficient takes maximum value for linear polarization in χ-ψ coordinate system: χ is the ellipticity angle and ψ is the orientation angle of polarization ellipse.

2. SCATTERING TYPES AND POLARIZATION SIGNATURES FOR THE UNSUPERVISED CLASSIFICATION BASED ON SCATTERING PROPERTIES

The classification method based on microwave scattering properties proposed by J. J. van Zyl classify the targets to

four scattering types [8]:

- Type 1: Odd number of reflections are distinguished at the target
- Type 2: Even number of reflections are distinguished at the target
- Type 3: Diffuse scattering are distinguished at the target
- Type 4: Others

For example, spheres and trihedral corner reflectors are classified into Type 1, dihedral corner reflectors are classified into Type 2, and forested areas are classified into Type 3, respectively. Furthermore, the surface of the sea that occurs Bragg scattering is classified into Type 1, buildings and the vegetation that occurs even number of reflections by trunk or stalk and the ground are classified into Type 2. This vegetation often grows vertically, and the polarization signature diagram has the peak at VV polarization. Mueller matrix for the typical dihedral corner reflector model is expressed as the equation (1), and the matrix for the conductor model placed vertically added to the dihedral corner reflector model is expressed in (2) [1][10].

$$[M] = \begin{bmatrix} 1 & 0 & 0 & 0 \\ 0 & 1 & 0 & 0 \\ 0 & 0 & -1 & 0 \\ 0 & 0 & 0 & -1 \end{bmatrix} \tag{1}$$

$$[M] = \begin{bmatrix} 0.75 & -0.25 & 0 & 0 \\ -0.25 & 0.75 & 0 & 0 \\ 0 & 0 & -0.5 & 0 \\ 0 & 0 & 0 & -0.5 \end{bmatrix} \tag{2}$$

The polarization signature diagrams made by these Mueller matrices are shown in Fig.1 respectively. From these diagrams, differences of the shape are shown.

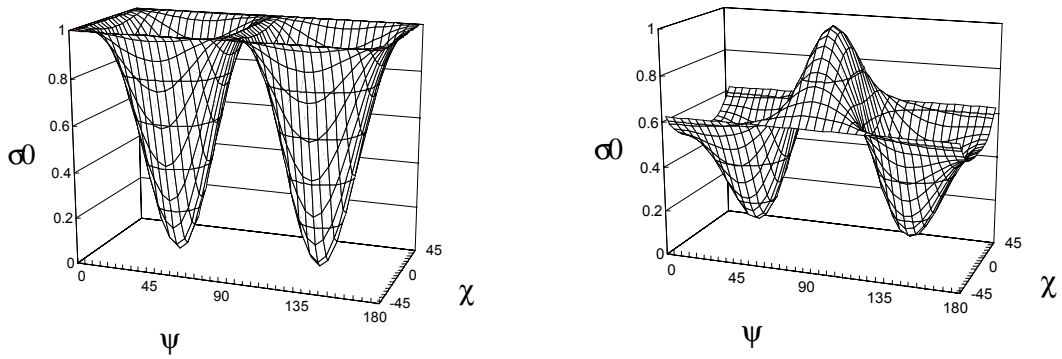

(a) typical dihedral corner reflector model (b) conductor model placed vertically added

Fig.1: Polarization signature diagrams made by the equation (1) and (2)

3. THE SHAPE FEATURE PARAMETER OF POLARIZATION SIGNATURE DIAGRAM

As the parameter that characterizes the shape of polarization signature diagram, the position in the coordinate system defined by ellipticity angle χ and orientation angle ψ for polarization ellipse where back-scattering coefficient has maximum value is proposed. Especially, the targets are classified by the orientation angle ψ in linear polarization. When we consider like polarization, ψ = 0 or 180 indicates HH polarization, and ψ = 90 indicates VV polarization. The equation to calculate back-scattering coefficient from Mueller matrix is expressed in (3) [1][4][10][11].

$$\sigma_0(\psi_r,\chi_r,\psi_t,\chi_t) = C\begin{bmatrix} 1 \\ \cos 2\psi_r \cos 2\chi_r \\ \sin 2\psi_r \cos 2\chi_r \\ \sin 2\chi_r \end{bmatrix}' \begin{bmatrix} m_{11} & m_{12} & m_{13} & m_{14} \\ m_{21} & m_{22} & m_{23} & m_{24} \\ m_{31} & m_{32} & m_{33} & m_{34} \\ m_{41} & m_{42} & m_{43} & m_{44} \end{bmatrix} \begin{bmatrix} 1 \\ \cos 2\psi_t \cos 2\chi_t \\ \sin 2\psi_t \cos 2\chi_t \\ \sin 2\chi_t \end{bmatrix} \quad (3)$$

where, the subscript t, r means that polarization t is transmitted and polarization r is used to receive the scattered waves. When like-polarization is considered, χ_t, ψ_t is equal to χ_r, ψ_r respectively. For linear polarization ($\chi = 0$), equation (3) can be rewritten as follows.

$$\sigma_0(\psi_r,\chi_r,\psi_t,\chi_t) = C\{m_{11} + \cos 2\psi(m_{21} + m_{12} + m_{22}\cos 2\psi + m_{32}\sin 2\psi) + \sin 2\psi(m_{31} + m_{13} + m_{23}\cos 2\psi + m_{33}\sin 2\psi)\} \quad (4)$$

If the radar is mono-static such as SIR-C, Mueller matrix is symmetrical, that is, $m_{ij} = m_{ji}$ ($i, j = 1, \ldots, 4$). In this case, σ_0 is

$$\sigma_0(\psi_r,\chi_r,\psi_t,\chi_t) = C\{m_{11} + \cos 2\psi(2m_{12} + m_{22}\cos 2\psi + m_{23}\sin 2\psi) + \sin 2\psi(2m_{13} + m_{23}\cos 2\psi + m_{33}\sin 2\psi)\} \quad (5)$$

Applying the element of Mueller matrix derived from each target into (5), the orientation angle ψ where σ_0 has maximum value can be found.

4. CLASSIFICATION ALGORITHM CONSIDERED THE SHAPE OF POLARIZATION SIGNATURE DIAGRAM

The classification method proposed in this study is constructed by two steps, the classification based on the scattering mechanism (STEP 1) and the classification based on the polarization in linear polarization where σ_0 has maximum value (STEP 2). In the first place, whole pixels are classified into four classes by J. J. van Zyl's algorithm. The next place, each pixel classified into scattering type 1, 2, and 3 is re-classified into three classes, σ_0 has maximum at HH polarization, VV polarization, and the others. That is, whole pixels are classified into 10 classes.

The proposed algorithm is illustrated as flow-chart in Fig.2. In STEP 1, each classified pixel is labeled any one from "1" to "4." In this step, labels correspond to the scattering types. In STEP 2, the classes are labeled from "11" to "33." The first letter of the label indicates the class number of STEP 1, and the second letter indicates the classification item of STEP 2. The second letter is labeled "1" if σ_0 has maximum at HH polarization, the second letter is labeled "2" if σ_0 has maximum at VV polarization, and the others are labeled "3."

5. CLASSIFICATION RESULTS BY SIR-C DATA

The data used in this study were obtained around Kashima, Japan, in 1994 by Shuttle Imaging Radar (SIR-C) on board the space shuttle "endeavor." SIR-C observed the earth using two kinds of wavelength band, L-band (wavelength was 24.0 cm) and C-band (wavelength was 5.66 cm). Main parameters for the data are listed in Table 1 [12].

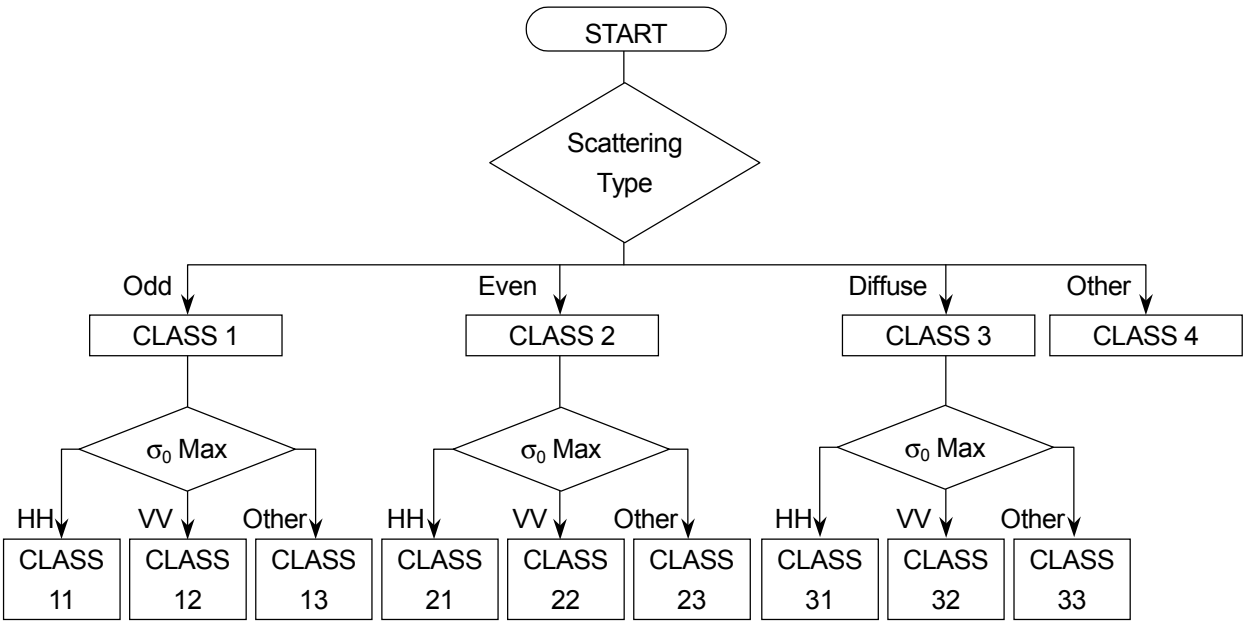

Fig.2: Flow-chart of proposed classification algorithm

Table 1: Main parameters of used data

Item	L-band	C-band
Wavelength	24.0 cm	5.66 cm
Data file No.	pr45511	pr45512
Data take No.	135.10	
Observation date	October 8, 1994	
Altitude of antenna	230 km	
Incident angle at image center	23.1 degree	
Range resolution	25.0 m	
Azimuth resolution	25.0 m	

Table 2: Sizes of extracted areas (unit: pixels)

Area	Azimuth	Range
Sea	80	100
Lake	100	90
Urban area	60	70
Paddy field	80	150
Grass field	25	90
Forested area	90	80

Fig.3 illustrates HH polarization images of the objective scene and the extracted areas. In this figure, (a) is the image of L-band data, and (b) is C-band. The bottom of this scene is Kashima Bay, and thick black line lying at upper part of the scene is Tone River. There is Sotonasakaura Lake in the center of this scene. The area among two rivers contains paddy field and grass field. Main analytical areas were extracted by the size shown in Table 3.

Comparing the classification results by L-band data with by C-band data, the results of L-band reflected more differences of targets. The tendency was seen in the results for STEP 2. Table 3 shows the classified rate of each class for extracted areas.

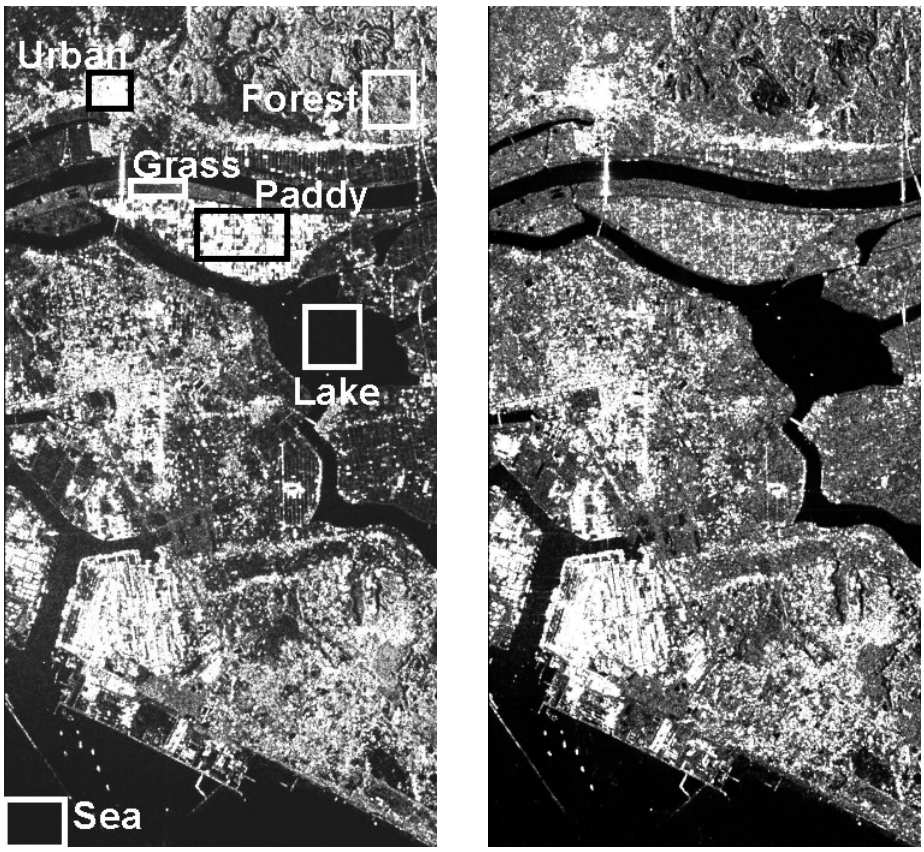

(a) L-band HH polarization (b) C-band HH polarization

Fig.3: Images of objective scenes and extracted areas

Table 3: Classification rate by L-band data of each class for extracted areas (unit: %)

Class No.	Sea	Lake	Urban	Paddy	Grass	Forest
1	99.66	91.15	16.10	14.62	20.89	33.35
2	0	4.19	58.40	79.74	4.71	3.44
3	0.34	4.66	25.31	5.64	72.22	60.36
4	0	0	0.19	0	2.18	2.85
11	0	0.29	6.29	2.93	5.87	8.67
12	92.84	90.62	2.52	11.02	4.49	2.40
13	6.83	0.24	7.29	0.67	10.53	22.28
21	0	0.22	44.33	12.65	2.62	1.78
22	0	3.97	3.93	67.05	1.60	1.29
23	0	0	10.14	0.04	0.49	0.38
31	0	0.06	11.81	0.67	20.62	15.79
32	0.34	4.60	2.33	4.60	7.02	3.71
33	0	0	11.17	0.38	44.58	40.86

In the classification result for STEP 1, water areas (sea and lake) had many pixels classified into scattering type1, urban area and paddy field had many type2 pixels. Many pixels classified into type3 were contained into forested area and grass field. For the results of L-band data, it is remarkable that urban area and paddy field were classified into separate classes when STEP 2 process was also performed. From this result, we can consider to combine the class 20 with urban area and to combine the class 21 with paddy field. However, more shape feature parameters are needed to separate other type targets.

6. CONCLUSIONS

In this study, J. J. van Zyl's unsupervised classification algorithm based on the scattering mechanism was expanded introducing the shape feature parameters of polarization signature diagrams. We proposed the orientation angle ψ of the polarization ellipse when back-scattering coefficient has maximum value in linear polarization. The proposed method was applied to SIR-C data, urban area and paddy field classified into the independent classes. Increasing the shape feature parameters, it will be able to classify the targets in detail.

ACKNOWLEDGMENT

The authors would like to thank Dr. Masaharu FUJITA, Professor of Tokyo Metropolitan Institute of Technology, Dr. Harunobu MASUKO and Dr. Tatsuharu KOBAYASHI, Senior research official of Communication Research Laboratory, offered the data of SIR-C.

REFERENCES

[1] F. T. Ulaby and C. Elachi: "Radar Polarimetry for Geoscience Applications," Artech House, Inc., 1990.

[2] H. A. Zebker and J. J. van Zyl: "Imaging Radar Polarimetry: A Review," Proc. IEEE, vol.79, no.11, pp.1583~1606, 1991.

[3] D. L. Evans, T. G. Farr, J. J. van Zyl, and H. A. Zebker: "Radar Polarimetry: Analysis Tools and Applications," IEEE Trans. Geoscience and Remote Sensing, vol.26, no.6, pp.774~789, 1988.

[4] O. Kobayashi and H. Hirosawa: "Radar Polarimetry – A New Measurement Technique in Microwave Remote Sensing –," J. RSSJ, vol.11, no.3, pp.127~133, 1991.

[5] J. S. Lee, M. R. Grunes, T. L. Ainsworth, L. J. Du, D. L. Schuler, and S. R. Cloude: "Un-supervised Classification Using Polarimetric Decomposition and the Complex Wishart Classifier," IEEE Trans. Geoscience and Remote Seinsing, vol.37, no.5, pp.2249~2257, 1999.

[6] T. Yamada and T. Hoshi: "Application of Polarization Signatures and Textural Features to Classification of Polarimetric SAR Images," Proc. The 2nd Magneto-Electronics International Symposium, pp.81~84, 1999.

[7] M. Hosokawa, Y. Ito, and T. Hoshi: "Extraction of Urban Characteristics using Polarimetric SAR Data and Self-Organizing Map," Trans. IEICE, vol.J84-B, no.6, pp.1043~1051, 2001.

[8] J. J. van Zyl: "Unsupervised Classification of Scattering Behavior Using Radar Polarimetry Data," IEEE Trans. Geoscience and Remote Sensing, vol.27, no.1, pp.36~45, 1989.

[9] T. Hoshi, T. Yamada, and M. Fujita: "Relationship between Wavelength and the Classification by Scattering Properties using SIR-C SAR Data," Proc. 1997 IEICE General Conference B1, p.217, 1997.

[10] Y. Yamaguchi: "Fundamentals of polarimetric radar and its applications," Realize Inc., 1998.

[11] J. J. van Zyl, H. A. Zebker, and C. Elachi: "Imaging radar polarization signatures: Theory and observation," Radio Science, vol.22, no.4, pp.529~543, 1987.

[12] R. L. Jordan, B. L. Huneycutt, and M. Werner: "The SIR-C/X-SAR Synthetic Aperture Radar System," Proc. IEEE, vol.79, no.6, pp.827~838, 1991.